the ice shelf base is the predominant phase change there, a conclusion that supports some earlier estimates from glaciological data (*1, 21*) and from laboratory and theoretical models (*12, 15a, 22*).

STANLEY S. JACOBS
ARNOLD L. GORDON, J. L. ARDAI, JR.
Lamont-Doherty Geological Observatory of Columbia University, Palisades, New York 10964

References and Notes

1. R. Thomas and P. Coslett, *Nature (London)* **228**, 47 (1970).
2. J. W. Clough and B. L. Hansen, *Science* **203**, 433 (1979). At J9, samples were obtained with modified water sampling bottles (General Oceanics) [E. Suckling, *Exposure* **3** (1975)], and from water pumped from several levels beneath the ice. Problems arising from slush ice and drilling fluid (Diesel Fuel Arctic) in the access hole lowered the quality of some salinity data. Several very low salinities near the ice shelf base are believed to have resulted from contamination from the hole, and are not reported. Temperature and depth observations were taken with low-range, deep-sea reversing thermometers.
3. In the Ross Sea, salinity-temperature-depth instruments (Plessey) were used; the data were corrected to simultaneous measurements obtained with water sampling bottles and thermometers [S. S. Jacobs, *Antarct. J. U.S.* **12**, 43 (1977); ———, P. Bruchhausen, J. Ardai, *ibid.*, in press].
4. S. S. Jacobs, A. F. Amos, P. M. Bruchhausen, *Deep-Sea Res.* **17**, 935 (1970).
5. P. Killworth, *ibid.* **21**, 815 (1974).
6. J. H. Zumberge and C. Swithinbank, *Antarct. Res. Geophys. Monogr. Am. Geophys. Union* **7**, 197 (1962).
7. U.S. Geological Survey, *Chart of the Ross Ice Shelf* (Department of the Interior, Washington, D.C., 1972).
8. E. Carmack and T. Foster, *Deep-Sea Res.* **22**, 77 (1975); A. Zverev, *Sov. Antarct. Exped. Inf. Bull.* **1**, 269 (1964).
9. A. E. Gilmour, *Science* **203**, 438 (1979).
10. I. A. Zotikov and V. Zagarodnov, unpublished data.
11. H. Ueda and D. Garfield, in *International Symposium on Antarctic Glaciological Exploration (ISAGE)*, A. J. Gow, C. Keeler, C. C. Langway, W. F. Weeks, Eds. (Hanover, N.H., 1968), pp. 53–68.
12. H. Wexler, *J. Glaciol.* **3**, 626 (1960).
13. C. Garrett, paper presented at the Joint Oceanographic Committee/Scientific Committee on Oceanic Research Conference on General Circulation models of the oceans and their relation to climate, Helsinki, 23 to 27 May 1977.
14. A. Foldvik and T. Kvinge, in *Polar Oceans*, M. Dunbar, Ed. (Arctic Institute of America, Calgary, 1977).
15. H. E. Huppert and J. S. Turner, *Nature (London)* **271**, 46 (1978).
15a. O. Pettersson, *Geogr. J.* **24**, 285 (1904); J. W. Sandstrom, in *Investigations in the Gulf of St. Lawrence and Atlantic Waters off Canada*, J. Hjort, Ed. (Department of Naval Service, Ottawa, 1919), p. 245.
16. V. Morgan, *Nature (London)* **238**, 393 (1972). The fabric, color, salty taste, and inclusions in the lower 6 m of an ice core obtained through the Ross Ice Shelf at J9 suggest a marine origin (I. Zotikov and J. Clough, by telegram to the University of Nebraska, 13 December 1978).
17. J. W. Clough, *Antarct. J. U.S.* **9**, 159 (1974).
18. A. Gordon, in "RISP science plan" (University of Nebraska, Lincoln, 1974), pp. 41–58.
19. C. Neal, paper presented at the Symposium on Dynamics of Large Ice Masses, Ottawa, 21 to 25 August 1978; *J. Glaciol.*, in press.
20. P. M. Bruchhausen, J. A. Raymond, S. S. Jacobs, A. L. DeVries, E. M. Thorndike, H. H. DeWitt, *Science* **203**, 449 (1979).
21. A. P. Crary, E. S. Robinson, H. F. Bennett, W. W. Boyd, Jr., *J. Geophys. Res.* **67**, 2791 (1962); P. A. Shumskiy and I. A. Zotikov, *UGGI, Assoc. Hydrol. Sci. Gen. Assembly Berkeley* (1963), pp. 225–231. Melting has also been calculated for the Erebus Glacier Tongue in McMurdo Sound [G. Holdsworth, *J. Glaciol.* **13**, 27 (1974)].
22. S. Martin and P. Kauffman, *J. Phys. Oceanogr.* **7**, 272 (1977).
23. K. Fujino, E. L. Lewis, R. G. Perkins, *J. Geophys. Res.* **79**, 1792 (1974).
24. We thank the personnel of U.S. Coast Guard icebreakers *Northwind* and *Burton Island*; Ross Ice Shelf Project drillers from Browning Engineering, the University of Nebraska, and the U.S. Army Cold Regions Research and Engineering Laboratory; and P. Bruchhausen, A. Amos, P. McDonald, and M. Rodman for field assistance. Several colleagues, in particular E. Molinelli, made helpful comments on the manuscript. This work was supported by NSF Office of Polar Programs grants C-726 to the University of Nebraska and 76-11872 and 77-22209 to Columbia University. Lamont-Doherty Geological Observatory contribution No. 2776.

12 July 1978; revised 26 September 1978

Ocean Tide and Waves Beneath the Ross Ice Shelf, Antarctica

Abstract. *The ocean tide in the southern Ross Sea is principally diurnal. The tropic tide range (double amplitude) is between 1 and 2 meters, depending on the location, and is closely related to the local water-layer thickness. The range of the tropic tide is more than three times the range of the equatorial tide. Cotidal and coamplitude charts were made for the largest diurnal constituents,* K_1 *and* O_1*, and a provisional cotidal map was made for the semidiurnal constituent* M_2*. The amplitudes of the diurnal tide constituents are larger in the Ross Sea than in the adjacent southern Pacific Ocean, indicating the existence of a diurnal resonance related to the shape and depth of the sea. Waves related to ocean swell propagate into the ice-covered region from the northern Ross Sea. These waves have amplitudes near 1 centimeter, and periods in the range 1 to 15 minutes. The speed at which these waves travel is successfully predicted by flexural wave theory.*

Tidal water movement beneath the Ross Ice Shelf causes diurnal changes in the elevation of the ice surface of as much as 2 m. Beginning in 1973, we undertook a study of the ocean tide in this region as part of the Ross Ice Shelf Project (RISP).

The Ross Sea is a marine embayment penetrating more than 1000 km into the Pacific sector of the Antarctic continent (Fig. 1). The southern part of this sea is covered by the Ross Ice Shelf, a tabular mass of floating ice that extends over about 560,000 km², and is almost everywhere 300 to 600 m thick. The thick ice cover presents an obstacle to the use of conventional tide gauges. In this study we used gravity meters to make measurements of the height of the ocean tide in an unusual way. Tidal fluctuations of

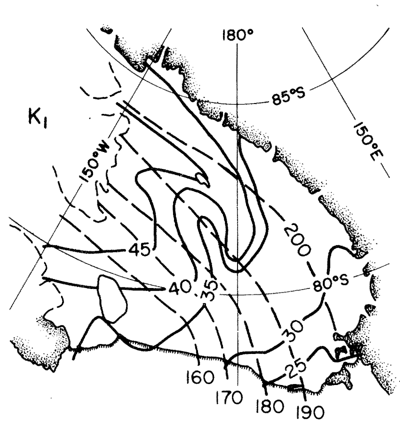

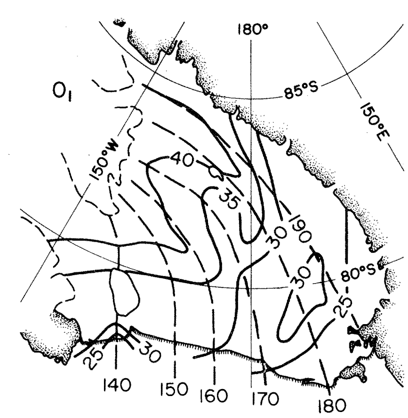

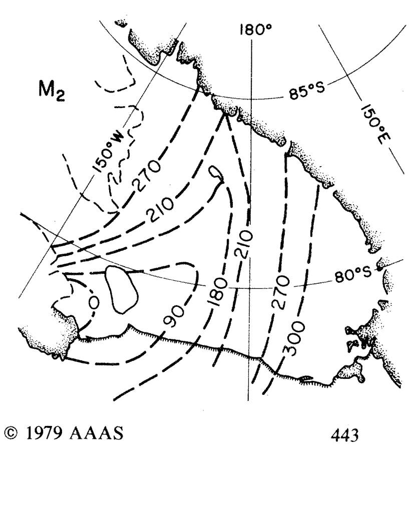

Fig. 1. Cotidal (dashed) and coamplitude (solid) contours of the K_1, O_1, and M_2 ocean tide constituents in the southern Ross Sea. Amplitudes are in centimeters and phases are in degrees relative to the Greenwich meridian. South is to the top; the ice-free part of the Ross Sea and the Pacific Ocean are to the bottom. The linear distance between 80°S and 85°S is 556 km.

0036-8075/79/0202-0443$00.50/0

the gravity at the surface of the ice shelf are related to tidal changes in the elevation and underlying water mass. During four austral summers, we operated Geodynamics model TRG-1 recording gravimeters at eight locations distributed over the study area, obtaining data for 29 to 58 days at each site. In addition, we have an earlier tidal gravity record from Little America V reported by Thiel *et al.* (*1*) and the results of tidal water-level measurements in McMurdo Sound near the northern boundary of the Ross Ice Shelf (*2*). All told, the principal characteristics of the ocean tide have been reliably determined at nine sites in the southern Ross Sea (Table 1). Because the ice shelf could be exploited as a floating platform, we had the unusual opportunity to make our tide measurements at selected locations over the study area. Elsewhere in the ocean the tide must be inferred largely from coastal measurements.

The measured tidal gravity variation results from a direct lunisolar effect and an ocean tide effect. The lunisolar effect is related to the masses and relative motions of the moon and sun with respect to the recording site, and in the Ross Ice Shelf region amounts to about 10 percent of the ocean tide effect. We corrected our data for the lunisolar effect by subtracting from our records the rigid-earth tide (*3*) increased by 16 percent to allow for the elastic yielding of the earth. (The error in this value of the correction is much less than the uncertainty of our basic measurement.) In the ocean tide effect, periodic changes in the thickness of the water layer beneath the ice shelf cause changes in the gravity field detected by a gravimeter. During high tide an additional mass of ocean water exists over a local region, and the related increase in elevation of the floating shelf causes a change in the gravity detected by a gravimeter on the surface. In converting the gravity change due to the ocean tide to an elevation change, we followed Thiel *et al.* (*1*), who showed that a change in water thickness beneath the ice, Δh, is related to a change in gravity at the surface, Δg, according to the expression Δh (meters) = $-3.7653\ \Delta g$ (milligals).

It is conventional to represent the tide by a sum of discrete harmonic constituents, which is different from a Fourier series in that it incorporates information about the tide-producing force. The tide records we obtained in connection with RISP were analyzed by the method described by Schureman (*4*). The time-independent amplitudes and phases of the harmonic constituents are summarized in Table 1. The level of uncertainty in our measurements can be inferred from high-resolution Fourier amplitude spectra of our field records. The amplitude spectra (*5*) indicate that the uncertainty in the values given in Table 1 is generally less than 2 cm for the RISP stations.

The analysis shows that the tide in the southern Ross Sea consists primarily of six harmonic constituents, of which the three largest have diurnal periods. The spatial variation of these constituents can be displayed by maps showing cotidal contours for the constituent phase and coamplitude contours for the amplitude. The constituent phase represents the lag of local constituent high water relative to the time of the maximum constituent equilibrium tide (*4*) on the meridian of Greenwich. The cotidal lines can also be viewed as the crest at different times of a fictitious ocean wave that would exist if only that particular constituent were disturbing the sea surface. Cotidal-coamplitude maps for the diurnal constituents K_1 and O_1 are shown in Fig. 1. For the semidiurnal constituent M_2 only the cotidal contours are mapped in Fig. 1.

The diurnal coamplitude contours are more detailed than if they were drawn by simple interpolation of the data from the nine sites. However, for these constituents a relationship between constituent amplitude and water-layer thickness was observed. This relationship is illustrated in Fig. 2, where curves were fitted to the data on the assumption that the phenomenon is analogous to the amplitude-depth relationship for a wave in a shallow canal of slowly varying depth. In such a canal, the wave amplitude is inversely proportional to the fourth root of the depth (*6*). For K_1 and O_1, proportionality constants

Table 1. Tidal harmonic constituents in the southern Ross Sea.

Site	Position	K_1		P_1		O_1		M_2		S_2		N_2	
		A*	P†	A	P	A	P	A	P	A	P	A	P
Base	82.5°S, 166.0°W	43	186	14	186	35	174	8	213	10	112	9	87
J9	82.4°S, 168.6°W	37	191	12	191	37	172	7	205	8	106	7	60
RI	80.2°S, 161.6°W	44	160	15	160	38	140	5	130	10	26	9	12
C36	79.8°S, 169.1°W	37	160	12	160	32	153	3	75	6	25	4	22
O19	79.6°S, 196.7°W	31	208	10	208	29	196	4	340	2	190	3	180
C16	81.2°S, 189.5°W	31	200	10	200	27	190	3	310	2	160	4	140
F9	84.3°S, 171.3°W	41	206	14	206	40	190	8	258	11	142	8	143
LAS‡	78.2°S, 162.3°W	34	154	11	154	25	141	3	35	5	342	5	344
McM§	77.9°S, 193.4°W	23	212	8	213	21	195	4	242	2	327	2	263

*Amplitude, in centimeters. †Phase angle, in degrees relative to the Greenwich meridian. ‡Little America V. §McMurdo Sound.

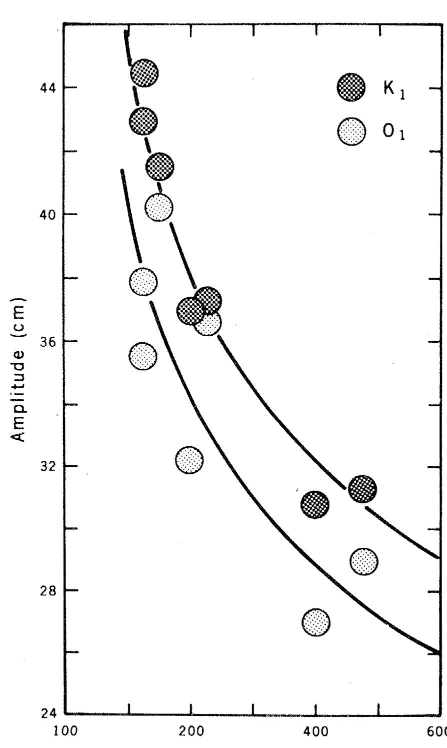

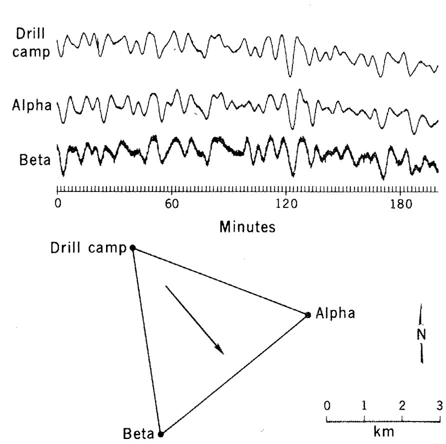

Fig. 2 (left). Comparison of K_1 and O_1 tidal amplitudes (A) in centimeters and water-layer thickness (h) in meters at seven sites on the Ross Ice Shelf. Curves have the form $A = bh^{-1/4}$, where b = 144 for the K_1 constituent and 129 for the O_1 constituent. Fig. 3 (right). Simultaneous 200-minute gravimeter records from three sites in a triangular array near site J9 display fluctuations produced by ocean waves. The vector shows the direction in which the flexural waves propagate across the array.

of 144 and 129, respectively, for amplitude in centimeters and depth in meters, yielded minimum root-mean-square errors of 1.0 and 2.4 cm. This observed relationship, together with a map of water-layer thickness beneath the ice shelf (*7*), was used to guide the location of the K_1 and O_1 coamplitude contours.

The spatial variation of the M_2 constituent is more complicated. The condition that our cotidal lines merge with the global M_2 cotidal chart of Zahel (*8*) requires a complex pattern of cotidal contours within the Ross Sea. The pattern presented in Fig. 1 displays no amphidromic points in the region, and none are definitely indicated by the amplitude data (Table 1). Other patterns requiring at least two amphidromic points in the Ross Sea are also consistent with Zahel's charts. For M_2 there is no simple relationship between amplitude and water-layer thickness. We would expect the complex cotidal contours to preclude a relationship analogous to the canal-type dependence observed for the diurnal constituents.

The ocean tide in the southern Ross Sea is dominated by the diurnal constituents. In this respect it is different from the tide in most parts of the world ocean, where the semidiurnal constituents are usually the largest. The range of tropic tide is between 1 and $1^1/_2$ m along the northern edge of the ice shelf, near 78°S, and increases to more than 2 m toward the southeast, near the Siple Coast. The equatorial range is generally less than one-third of the tropic range. The amplitudes of the diurnal constituents, particularly K_1 and O_1, are too large to be explained simply in terms of the lunisolar tide-raising force [equilibrium tide theory (*4*)]. They are also larger than might be anticipated from their amplitudes in the southern Pacific Ocean (*9*). Thus a diurnal resonance related to the shape of the embayment and the water depth is indicated. The wavelengths of the diurnal constituents are seen (Fig. 1) to be approximately four times the length of the Ross Sea, measured in the direction of a progressing tide from the edge of the continental shelf. This is a condition for diurnal resonance.

Waves having periods in the range 1 to 15 minutes and amplitudes near 1 cm are superposed on the tidal water-level fluctuations beneath the Ross Ice Shelf (*5*). These waves appear on the tidal gravity records from all our recording sites. On our field records the dominant wave periods are between 1 and 2 minutes near the northern margin of the ice shelf. The waves are attenuated with increasing distance from open water, and the shorter periods are attenuated relatively rapidly so that in the region farther south than 84°S the dominant period is near 10 minutes.

To obtain data on the speed and direction of propagation of these waves, we operated three gravimeters simultaneously in a 5-km triangular array near site J9 (Table 1). From 22 to 26 November 1977 we obtained more than 38 hours of simultaneous data in five segments, varying in length from $2^1/_2$ to 16 hours. These data were digitally recorded at 4-second intervals by microprocessor-based digitizers of our own design. Before the 1977–1978 season, our data were recorded on strip-chart recorders having a paper speed of 1 inch per hour, and data in the period range 1 to 15 minutes were not well recorded. Figure 3 shows 200-minute segments from the three gravimeter records and the orientation of the array.

We calculated the wave speed and direction from the time offsets of the wave between the three recording sites. The time shifts along each leg of the array were determined by cross-correlating the simultaneous record segments from the two stations on the leg. We found the wave speed to be 57 ± 11 m/sec and the wave direction to be N139°E ± 10° (Fig. 3). The wave speed is consistent with the speed of a flexural wave (*10*), given the ice and water-layer thickness at site J9. For wave periods greater than 9 minutes this speed is the same as the shallow-water gravity wave speed, and is 48.3 m/sec for the 238-m water thickness at J9. The influence of the ice layer increases the flexural wave speed to 50.5 m/sec at the 6-minute period, and 62.5 m/sec at the 3-minute period. We found that our data were not adequate to resolve the subtle difference in wave speed at different periods in the range 3 to 9 minutes, but the value of 57 m/sec that we measured is appropriate as an average for the periods evident on the records (Fig. 3). The direction of propagation is consistent with the supposition that the flexural waves are excited at the ice front by infragravity waves in the open ocean north of the ice shelf.

RICHARD T. WILLIAMS
EDWIN S. ROBINSON
Department of Geological Sciences, Virginia Polytechnic Institute and State University, Blacksburg 24061

References and Notes

1. E. C. Thiel, A. P. Crary, R. A. Haubrich, J. C. Behrendt, *J. Geophys. Res.* **65**, 629 (1960).
2. R. A. Heath, *N.Z. J. Mar. Freshwater Res.* **3**, 376 (1971).
3. I. M. Longman, *J. Geophys. Res.* **64**, 2351 (1959).
4. P. W. Schureman, *Manual of Harmonic Analysis and Prediction of Tides* (Special Publication 98, U.S. Coast and Geodetic Survey, Rockville, Md., rev. ed., 1940).
5. E. S. Robinson, R. T. Williams, H. A. C. Neuburg, C. S. Rohrer, R. L. Ayers, *Ann. Geophys.* **33**, 147 (1977).
6. H. Lamb, *Hydrodynamics* (Dover, New York, 1932), p. 273.
7. L. L. Greischar and C. R. Bentley, *Eos* **59**, 309 (1978).
8. W. Zahel, *Mitt. Inst. Meereskd. Univ. Hamburg No. 17* (1970).
9. K. C. Tyrone, Y. Sergeev, A. Michurin, *Vestn. Leningr. Univ. No. 24* (1967); K. T. Bogdanov, *Marées Terr. Bull. Inf. Belg. R. Obs.* **67**, 3712 (1973).
10. M. Ewing, A. P. Crary, A. M. Thorne, *Physics (N.Y.)* **5**, 181 (1934); D. H. Clements, D. E. Willis, J. T. Wilson, *Report of Project Michigan. Waves in Lake Ice from Impacts* (Willow Run Laboratories, University of Michigan, Ann Arbor, 1958).
11. Supported by NSF grants GV-40434 and DPP-73-05873.

14 June 1978; revised 2 October 1978

Tritium and Carbon-14 Distributions in Seawater from Under the Ross Ice Shelf Project Ice Hole

Abstract. *The tritium and carbon-14 activities of seawater samples collected from 22 to 200 meters below the ice at the Ross Ice Shelf Project ice hole are reported. The tritium results show that the waters below the ice have exchanged with Ross Sea water since the advent of nuclear testing. The carbon-14 results indicate that waters in the upper layer exchange in time periods of less than 6 years. Measurements of these isotopes in seawater under the Ross Ice Shelf in McMurdo Sound show that this water has a different history.*

Tritium and carbon-14 were introduced into the atmosphere in major quantities as a result of nuclear weapons testing in the early 1960's. Tritium (half-life, $t_{1/2}$ = 12.3 years) is a valuable tracer since it is a radioactive isotope of hydrogen and will follow the path of water exactly in the world ocean (*1*). There are no particulate or biological effects that will alter tritium concentrations in seawater. The natural concentrations of tritium present before the bomb tests are negligible as compared to the amounts produced by weapons testing and can be ignored (*2*). Tritium concentrations attained a maximum of 1 to 2 tritium units [1 TU is one tritium atom per 10^{18} hydrogen (protium) atoms] in the late 1960's and early 1970's and have been decreasing since then. Tritium found in seawater

0036-8075/79/0202-0445$00.50/0